Surface ablation of corneal stroma with few-cycle laser pulses at 800 nm

L. Hoffart,[1] P. Lassonde,[2] F. Légaré,[2] F. Vidal,[2,*] N. Sanner,[3] O. Utéza,[3] M. Sentis,[3] J.-C. Kieffer,[2] and I. Brunette[4]

[1]Département d'Ophtalmologie, Université de la Méditerranée, Marseille, France
[2]Institut National de la Recherche Scientifique – Énergie, Matériaux et Télécommunications, 1650, boulevard Lionel-Boulet, Varennes, QC, J3X 1S2, Canada
[3]Laboratoire LP3, UMR 6182 CNRS – Université de la Méditerranée, C. 917, 163, Avenue de Luminy, 13288 Marseille, cedex 9, France
[4]Department of Ophthalmology, University of Montreal, Maisonneuve-Rosemont Hospital Research Center, 5415, L'Assomption boulevard, Montreal, QC, H1T 2M4, Canada
**vidal@emt.inrs.ca*

Abstract: We report measurements of crater diameter and surface ablation threshold as a function of laser fluence in porcine corneal stroma and fused silica with pulse durations of 7 fs (2.7 optical cycles), 30 fs and 100 fs at 800 nm. For laser pulses with Gaussian radial intensity profile, we show experimentally that the square of the crater diameter is a linear function of the logarithm of the fluence in fused silica, while it is closer to a linear function of the fluence in corneal stroma. Extrapolating these relations to zero diameter indicates that for both media the minimum fluence required for surface ablation is reduced with shorter pulse duration. A simple theoretical model suggests that this effect is due to a more significant contribution of photoionization as the laser pulse duration shortens.

©2010 Optical Society of America

OCIS codes: (170.1020) Ablation of tissue; (170.3660) Propagation of light in tissue; (160.4890) Organic materials.

References and links

1. M. Han, L. Zickler, G. Giese, M. Walter, F. H. Loesel, and J. F. Bille, "Second-harmonic imaging of cornea after intrastromal femtosecond laser ablation," J. Biomed. Opt. **9**(4), 760–766 (2004).
2. T. Juhasz, F. H. Loesel, R. M. Kurtz, C. Horvath, J. F. Bille, and G. Mourou, "Corneal refractive surgery with femtoseconds lasers," IEEE J. Sel. Top. Quantum Electron. **5**(4), 902–910 (1999).
3. M. Han, G. Giese, L. Zickler, H. Sun, and J. F. Bille, "Mini-invasive corneal surgery and imaging with femtosecond lasers," Opt. Express **12**(18), 4275–4281 (2004).
4. M. Niemz, *Laser-Tissue Interactions-Fundamentals and Applications*, 3rd edition (Springer Press, Heidelberg, 2003).
5. J. F. Bille, C. Harner, and F. H. Loesel, *New Frontiers in Vision and Aberration-Free Refractive Surgery* (Springer Press, Heidelberg, 2002).
6. K. König, B. Wang, I. Riemann, and J. Kobow, "Cornea surgery with nanojoule femtosecond laser pulses," Proc. SPIE **5688**, 288–293 (2005).
7. S. Macrae, "Thin-flap femtosecond LASIK," J. Refract. Surg. **26**(7), 469–470 (2010).
8. P. S. Binder, "Femtosecond Applications for Anterior Segment Surgery," Eye Contact Lens, Epub ahead of print, Aug 10 (2010).
9. A. Ertan, and J. Colin, "Intracorneal rings for keratoconus and keratectasia," J. Cataract Refract. Surg. **33**(7), 1303–1314 (2007).
10. L. Hoffart, H. Proust, F. Matonti, B. Ridings, and J. Conrath, "Short-term results of penetrating keratoplasty performed with the Femtec femtosecond laser," Am. J. Ophthalmol. **146**(1), 50–55 (2008).
11. P. Maier, F. Birnbaum, and T. Reinhard, "Therapeutischer Einsatz des Femtosekundenlasers in der Hornhautchirurgie," Klin. Monatsbl. Augenheilkd. **227**(06), 453–459 (2010).
12. M. Farid, and R. F. Steinert, "Femtosecond laser-assisted corneal surgery," Curr. Opin. Ophthalmol. **21**(4), 288–292 (2010).
13. S. K. Choi, D. Lee, J. H. Kim, and S. H. Oh, "A novel technique: eccentric lamellar keratolimbal allografting using a femtosecond laser," Cornea **29**(9), 1062–1065 (2010).
14. J. G. Fujimoto, W. Z. Lin, E. P. Ippen, C. A. Puliafito, and R. F. Steinert, "Time-resolved studies of Nd:YAG laser-induced breakdown. Plasma formation, acoustic wave generation, and cavitation," Invest. Ophthalmol. Vis. Sci. **26**(12), 1771–1777 (1985).

#134586 - $15.00 USD Received 7 Sep 2010; revised 8 Nov 2010; accepted 8 Nov 2010; published 22 Dec 2010
(C) 2011 OSA

15. A. Vogel, W. Hentschel, J. Holzfuss, and W. Lauterborn, "Cavitation bubble dynamics and acoustic transient generation in ocular surgery with pulsed neodymium: YAG lasers," Ophthalmology **93**(10), 1259–1269 (1986).
16. T. Juhasz, G. A. Kastis, C. Suárez, Z. Bor, and W. E. Bron, "Time-resolved observations of shock waves and cavitation bubbles generated by femtosecond laser pulses in corneal tissue and water," Lasers Surg. Med. **19**(1), 23–31 (1996).
17. T. Juhasz, X. H. Hu, L. Turi, and Z. Bor, "Dynamics of shock waves and cavitation bubbles generated by picosecond laser pulses in corneal tissue and water," Lasers Surg. Med. **15**(1), 91–98 (1994).
18. F. H. Loesel, A. Tien, S. Backus, H. Kapteyn, M. Murnane, R. M. Kurtz, S. Sayegh, and T. Juhasz, "Effect of reduction of laser pulse width from 100 ps to 20 fs on the plasma-mediated ablation of hard and soft tissue," Proc. SPIE **3565**, 116–123 (1998).
19. R. M. Kurtz, X. Liu, V. M. Elner, J. A. Squier, D. Du, and G. A. Mourou, "Photodisruption in the human cornea as a function of laser pulse width," J. Refract. Surg. **13**(7), 653–658 (1997).
20. D. Giguère, G. Olivié, F. Vidal, S. Toetsch, G. Girard, T. Ozaki, J. C. Kieffer, O. Nada, and I. Brunette, "Laser ablation threshold dependence on pulse duration for fused silica and corneal tissues: experiments and modeling," J. Opt. Soc. Am. A **24**(6), 1562–1568 (2007).
21. N. Sanner, O. Utéza, B. Chimier, M. Sentis, P. Lassonde, F. Légaré, and J. C. Kieffer, "Toward determinism in surface damaging of dielectrics using few-cycle laser pulses," Appl. Phys. Lett. **96**(7), 071111 (2010).
22. M. Nisoli, S. De Silvestri, O. Svelto, R. Szipöcs, K. Ferencz, C. Spielmann, S. Sartania, and F. Krausz, "Compression of high-energy laser pulses below 5 fs," Opt. Lett. **22**(8), 522–524 (1997).
23. J. M. Liu, "Simple technique for measurements of pulsed Gaussian-beam spot sizes," Opt. Lett. **7**(5), 196–198 (1982).
24. M. Lenzner, J. Krüger, S. Sartania, Z. Cheng, C. Spielmann, G. Mourou, W. Kautek, and F. Krausz, "Femtosecond optical breakdown in dielectrics," Phys. Rev. Lett. **80**(18), 4076–4079 (1998).
25. G. Olivié, D. Giguère, F. Vidal, T. Ozaki, J. C. Kieffer, O. Nada, and I. Brunette, "Wavelength dependence of femtosecond laser ablation threshold of corneal stroma," Opt. Express **16**(6), 4121–4129 (2008).
26. D. Strickland, and G. Mourou, "Compression of amplified chirped optical pulses," Opt. Commun. **55**(6), 447–449 (1985).
27. N. Sanner, O. Uteza, B. Bussiere, G. Coustillier, A. Leray, T. Itina, and M. Sentis, "Measurement of femtosecond laser-induced damage and ablation thresholds in dielectrics," Appl. Phys., A Mater. Sci. Process. **94**(4), 889–897 (2009).
28. E. Goulielmakis, M. Schultze, M. Hofstetter, V. S. Yakovlev, J. Gagnon, M. Uiberacker, A. L. Aquila, E. M. Gullikson, D. T. Attwood, R. Kienberger, F. Krausz, and U. Kleineberg, "Single-cycle nonlinear optics," Science **320**(5883), 1614–1617 (2008).
29. F. Reiter, U. Graf, M. Schultze, W. Schweinberger, H. Schroder, N. Karpowicz, A. M. Azzeer, R. Kienberger, F. Krausz, and E. Goulielmakis, "Generation of sub-3 fs pulses in the deep ultraviolet," Opt. Lett. **35**(13), 2248–2250 (2010).
30. C. Vozzi, F. Calegari, E. Benedetti, S. Gasilov, G. Sansone, G. Cerullo, M. Nisoli, S. De Silvestri, and S. Stagira, "Millijoule-level phase-stabilized few-optical-cycle infrared parametric source," Opt. Lett. **32**(20), 2957–2959 (2007).
31. M. Giguère, B. E. Schmidt, A. D. Shiner, M.-A. Houle, H.-C. Bandulet, G. Tempea, D. M. Villeneuve, J.-C. Kieffer, and F. Légaré, "Pulse compression of submillijoule few-optical-cycle infrared laser pulses using chirped mirrors," Opt. Lett. **34**(12), 1894–1896 (2009).

1. Introduction

Recently, femtosecond laser technology has revolutionized the field of eye surgery, particularly corneal surgery, providing the advantages of combined high ablation precision and minimized collateral tissue damage [1–6]. Femtosecond lasers are used in refractive surgery for creation of laser in situ keratomileusis (LASIK) flap [7,8], for the dissection of intrastromal channels for intracorneal ring segments implantation in keratoconus eyes [9], for the trephination of donor and recipient buttons in penetrating keratoplasty [10] and for stromal dissection in lamellar keratoplasty [11–13]. The femtosecond laser wavelength used for intrastromal dissection is much longer (about 1 micrometer) than that of the excimer laser used for surface reshaping (193 nm) because the laser must pass through the cornea without damaging the tissue until it reaches a specific point. Today, the challenge in femtosecond laser dissection is to optimize clinical operating conditions, for maximal precision and minimal damage to surrounding corneal tissues.

Focusing the femtosecond laser beam into the corneal tissue induces optical breakdown and the generation of a plasma through nonlinear absorption [14]. Expansion of the cavitation bubble dissects and ablates the tissue. Associated shockwaves and heat dissipation, however, may result in collateral tissue damage [15,16]. Lowering the femtosecond laser pulse energy allows to decrease the amount of energy deposited into the tissue, the shock wave amplitude, and the cavitation bubble size [17,18]. Smaller ablation spots can then be scanned closer,

#134586 - $15.00 USD Received 7 Sep 2010; revised 8 Nov 2010; accepted 8 Nov 2010; published 22 Dec 2010
(C) 2011 OSA

allowing for greater precision and smoother intrastromal dissection at the microscopic scale, two key parameters in corneal surgery. Those are the motivations to study corneal laser ablation with forefront femtosecond few-cycle laser technology.

Within the recent years, laser pulse duration down to 20 fs were shown to yield lower ablation thresholds in corneal tissues [18–20]. Therefore, one expects that extremely short pulses, such as few optical cycle pulses, would decrease further the ablation threshold and thus reduce even more the collateral tissue damage. With the advances of ultrafast optics, intense femtosecond laser pulses are now available to study tissue ablation mechanisms in the few-cycle regime (1 optical cycle = 2.6 fs at 800 nm). Using this few-cycle technology [22], we report on the surface ablation threshold as a function of laser pulse duration of pig corneal stroma with, to our knowledge, the shortest pulse duration in the available literature on corneal ablation. We used a single laser system to produce pulse durations of 7 fs (2.7 optical cycles), 30 fs and 100 fs at 800 nm, thus avoiding the deviations resulting from using different laser beam parameters.

The method we used to determine the threshold fluence consists in extrapolating the measurements of the crater diameters squared as a function of the laser fluence to the point where the diameter vanishes [23]. The craters were produced by single laser shot. For the sake of comparison and to validate the method and experimental setup, we also investigated ablation of polished fused silica samples. Surface ablation threshold of fused silica was determined previously by Lenzner *et al*. down to 5 fs [24] and more recently by Sanner *et al.* down to 7 fs [21]. The method used in [24] was also an extrapolation method, with the difference that the extrapolated quantity was the volume of the craters produced by 50 laser shots, instead of their diameter squared. In [21] the authors used a probabilistic approach based on the observation or not of a damage at the surface of the sample after performing many laser shots around the threshold fluence.

This paper is organized as follows. In the next section, we describe the experimental setup and methodology used to measure the surface ablation threshold dependence on the pulse duration. We then present the experimental results for corneal stroma and fused silica. In that section, we also discuss the results in the light of a theoretical model presented in a previous work [25]. The last section concludes the paper.

2. Materials and methods

A schematic overview of the experimental setup is shown in Fig. 1. The laser system is based on the chirped pulse amplification technique [26] and uses Ti-Sapphire multi-pass amplification (RedDragon, KMLabs, Boulder, USA). It can deliver pulse duration down to 30 fs, with 4.5 mJ of energy per pulse at a repetition rate of 5 kHz. The spatial intensity distribution of the amplified beam was measured to be close to the ideal TEM_{00} mode (Gaussian). For further pulse compression, we used the standard approach based on spectral broadening through nonlinear propagation in a hollow core fiber (HCF) filled with noble gas and dispersion compensation with chirped mirrors [22].

Briefly, the amplified 30 fs pulses were coupled to an argon-filled HCF using a f = 1 m plano-convex UV fused silica lens. Using 0.3 mJ of energy per pulse, we were able to generate broadband spectra enabling Fourier transform-limited pulse duration of 7 fs. Typical transmission of the HCF setup was 50%. Recollimation of the laser beam was achieved using a f = 1.5 m plano-concave silver mirror. After the HCF setup, the laser beam was reflected on a pair of germanium plates installed at Brewster angle (reflective polarizer). The energy per pulse was accurately controlled using a half-waveplate installed before the HCF. The 7-fs pulses were obtained by reflecting the laser beam on a pair of commercially available chirped mirrors (Femtolasers, Vienna, Austria). For 30 fs pulse generation and longer, helium was used instead of argon to fully suppress the spectral broadening while maintaining the input pulse duration. The 100 fs pulses were generated by reducing the spectral bandwidth of the laser pulses in the grating compressor of the Ti-Sapphire amplifier. The laser pulse duration was measured using an interferometric autocorrelator designed to characterize pulse duration down to 5 fs (Femtolasers, Vienna, Austria).

#134586 - $15.00 USD Received 7 Sep 2010; revised 8 Nov 2010; accepted 8 Nov 2010; published 22 Dec 2010
(C) 2011 OSA

Single-pulse energies were obtained from the measurement of the average output power of the 5 kHz pulse trains by placing a photodetector (Model PH100-si, Gentec Electro-Optics, Québec, Canada) in front of the beam. The pulse to pulse energy variation was controlled by a photodiode and was less than 3% RMS. The energy on the sample surface was varied from 0.1 to 2.7 μJ during the experiments. The laser pulse was focused on the sample surface by a gold-plated parabolic mirror with an effective focal length of 50.8 mm, at an angle normal to the target surface. The sample was installed on a XYZ translation stage and the tissue surface was translated along the optical axis prior to the measurements to ensure that the focal plane of the focusing mirror coincides with the tissue surface. Accurate focusing of the beam on the sample surface was achieved by monitoring the transmission signal using a photodiode (DET10A, Thorlabs, Newton, New Jersey, USA). When a significant decrease of this signal resulting from a plasma formation at the focal point was observed, we considered that the beam was focused on the cornea surface. This procedure was done at the lowest possible energy to yield the best accuracy in positioning the sample with respect to the focal plane. Then, the sample was rapidly moved perpendicular to the optical axis to ensure single shot ablation.

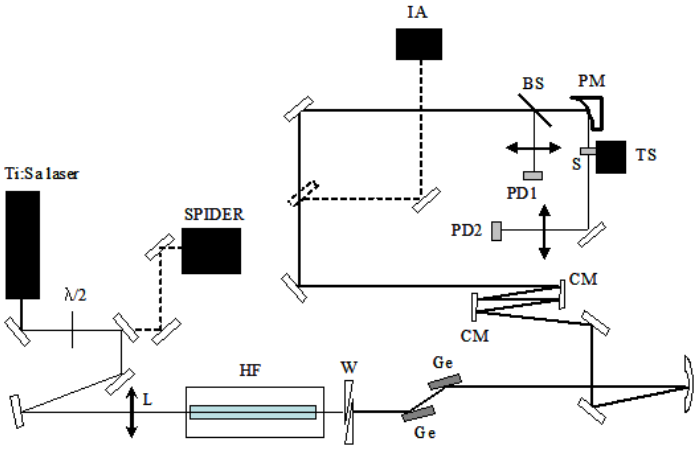

Fig. 1. Experimental set-up: BS: beam splitter; CM: chirped mirrors; Ge: Germanium plates; HF: hollow-core fiber; IA: interferometric autocorrelator; $\lambda/2$: half-wave plate; L: f = 1m lens; PD: photodiode; PM: 90° off-axis parabolic mirror; S: sample; TS: translation stage; W: wedges

In order to measure the spot size and to control the beam quality, the focal plane was imaged onto a CCD camera (Spiricon LBA-FW-SCOR20, Logan, USA) and analyzed with a beam profiler software. The focal spot diameter was defined as the diameter D_0 at $1/e^2$ of the maximum intensity. The laser fluence F (energy per unit area) was obtained from the laser beam energy E through the relation $F = 8E/\pi D_0^2$. It is worth noting that this definition is the most appropriate for the extrapolation method used to determine the threshold fluence since F coincides with the fluence at the peak of the pulse, i.e. at zero diameter.

The crater diameters were deduced from the visible damage area by using a 50 × reflection mode optical microscope (Reichert MEF4M, Wetzlar, Germany). Photos were taken using a digital acquisition system (LEICA DFC-320, Wetzlar, Germany) and the crater diameters D was measured by image analysis (ImagePro Discovery, Media Cybernetics, Bethesda, USA). We started the surface ablation threshold measurements from the highest fluence, progressively decreasing the laser energy until damages became no longer visible on the surface of the sample. Threshold measurements were performed at 7 fs, 30 fs and 100 fs pulse duration on fresh porcine eyes and fused silica samples.

#134586 - $15.00 USD Received 7 Sep 2010; revised 8 Nov 2010; accepted 8 Nov 2010; published 22 Dec 2010
(C) 2011 OSA

(a) Fused silica

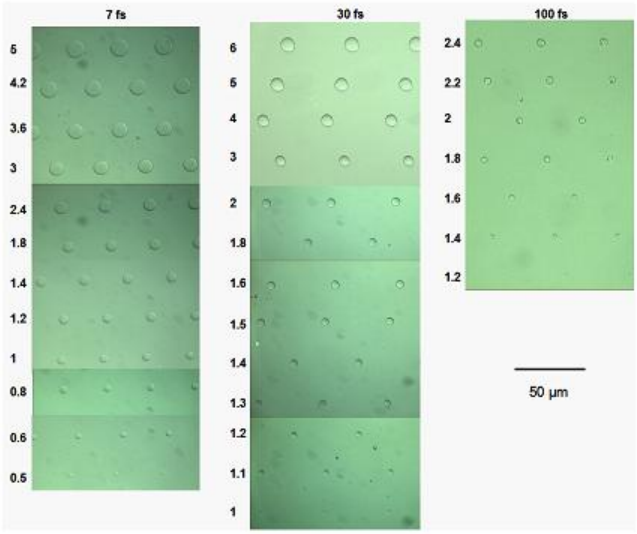

(b) Corneal stroma

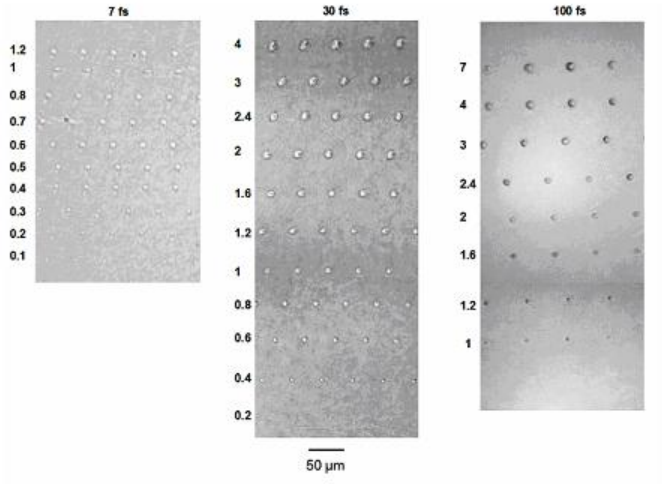

Fig. 2. Pictures of the craters produced in (a) fused silica using a 50 × microscope and (b) corneal stroma using a 20 × microscope, for three pulse durations and for several laser energies (left scale in µJ).

We used 2 mm-thick high-purity superpolished amorphous fused silica samples (Suprasil 2 from Heraeus Quarzglas, Hanau, Germany) with impurity < 0.065 ppm and residual roughness 0.2 nm measured by AFM. The fresh porcine eyes were obtained from a slaughterhouse and preserved at 4 °C in plastic bags until the experiments, which were performed within 8 hours after death. Just before the femtosecond laser ablation, the corneal epithelium was gently removed (blade #15, Albion surgicals, Sheffield England), the corneoscleral button was dissected and full thickness corneal layers (3 mm wide, from limbus to limbus) were prepared and gently laid flat on a glass slide, with the stromal side exposed to the laser beam. Tissue hydration was maintained by regular (about every 3 minutes)

#134586 - $15.00 USD Received 7 Sep 2010; revised 8 Nov 2010; accepted 8 Nov 2010; published 22 Dec 2010
(C) 2011 OSA

instillation of a balanced salt solution drop. During laser experiments, irrigation was suspended to avoid any excess liquid that could interfere with the measurements. After laser experimentation, the corneal specimens are immediately examined under the microscope.

3. Results and discussion

3.1 Shape of the craters

Examples of craters produced at the surface of fused silica and corneal stroma are shown in Fig. 2. Figure 2(a) shows craters produced in fused silica for laser energy between 0.5 and 6 μJ, corresponding to a fluence range of ~1.5 – 19.3 J/cm^2. For 7 and 30 fs pulses, the craters are circular (as expected for the TEM_{00} mode), with well-defined edges, while for the 100 fs pulses the edges are rougher. This roughness may result from thermal damage or from redeposition of ablated material near the crater rim.

Figure 2(b) shows the corresponding pictures for stroma, but on a larger energy range (between 0.1 and 7 μJ, i.e., between 0.3 and 22 J/cm^2). One first notices that the craters remain visible for smaller energies when the pulse duration decreases. A main difference with respect to the craters of Fig. 2(a) for fused silica is their irregular shape, especially for 7 fs and 30 fs pulses for the highest energies shown, although the same laser conditions were used for both materials. For craters with irregular shapes, we made an average between the largest and smallest diameters. Another difference with respect to the craters produced in fused silica is the presence of a small off-centered "dark spot" inside many craters, as can be seen in the 30 fs case of Fig. 2(b). It is not clear yet if those "dark spots" are a mere optical effect or if they are related to actual changes in the material. For the diameter measurements, we thus considered only the outer rim of the craters.

3.2 Determination of threshold fluence

Assuming that the crater rim corresponds to a threshold fluence $F_{th} = \Delta E / \Delta S$, where ΔE is the laser energy contained in the thin ring between the diameters D and $D + \Delta D$, and ΔS is the area of the ring, we find that for a Gaussian intensity profile pulse with a diameter D_0 at $1/e^2$ of the peak, the crater diameter is given by the relation:

$$D^2 = \frac{1}{2} D_0^2 \left(\ln F - \ln F_{th} \right) \qquad (1)$$

Therefore, under this assumption, extrapolating a plot of D^2 vs ln F to $D^2 = 0$ provides the threshold fluence F_{th} [27]. The plots for 7 fs, 30 fs and 100 fs pulse durations are shown in Fig. 3 for the fused silica targets. The fluence was defined using the selected beam energy and beam diameter D_0, measured using the CCD camera, as explained above. The linear regression curves were performed over the whole set of measurements for a given pulse duration. Table 1 shows the linear regression coefficients with their associated standard error and correlation coefficient R characterizing the fit quality. Both the coefficients R in Table 1 and visual inspection of Fig. 3 indicate that Eq. (1) is well verified. Moreover, the slopes B of the regression curves for D^2 vs log F (where log denotes the base 10 logarithm) are in good agreement with the values $\ln(10) D_0^2 / 2$ calculated using the independent measurements of the beam diameter D_0 (also given in Table 1). The values of D_0 calculated by the two methods coincide within the error bars, except for the 30 fs case, where the value obtained from B is too large by about 11% (9.9 ± 0.2 μm). It is worth noting that the crater diameters for the 7 fs pulse as a function of the fluence do not show any distinctive features when compared to the multi-cycle pulses of 30 fs and 100 fs. Therefore, the assumptions leading to Eq. (1) seem to be verified for all pulse durations in the case of fused silica.

#134586 - $15.00 USD Received 7 Sep 2010; revised 8 Nov 2010; accepted 8 Nov 2010; published 22 Dec 2010
(C) 2011 OSA

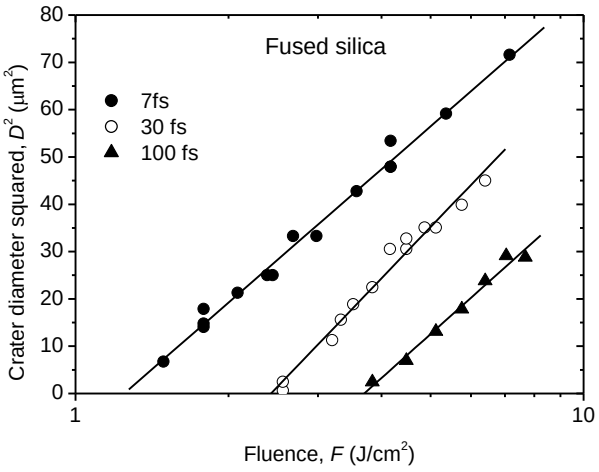

Fig. 3. Crater diameter squared as a function of laser fluence for fused silica. Lines were obtained by linear regression of the measurements.

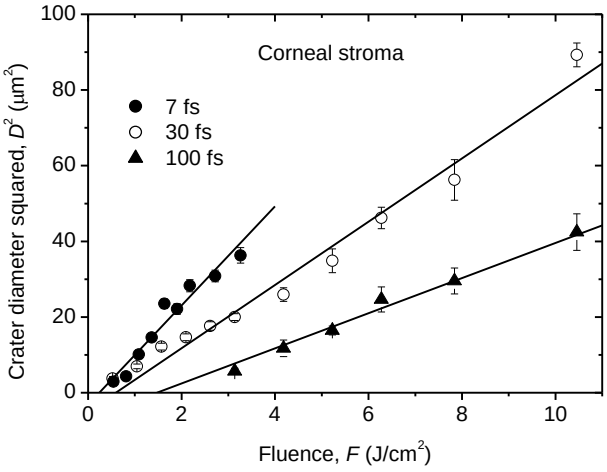

Fig. 4. Crater diameter squared as a function of laser fluence for corneal stroma. The dots are the mean values of several measurements and the vertical error bars are estimates of the standard errors of the mean values. Lines were obtained by linear regression of the full set of measurements for all pulse durations.

When applying the same methodology to corneal stroma, two striking differences appeared with respect to fused silica. First, we found much larger standard deviations of the diameter measurements than for fused silica for a given fluence and pulse duration. This is likely due to the higher roughness and lower homogeneity of this material on the scale length of the laser beam diameter (about 10 microns). Therefore, to obtain statistically meaningful data, we performed about 200 diameter measurements for all pulse durations using three different cornea samples. The second main difference observed with respect to fused silica was that Eq. (1) is not well verified for stroma. Indeed the values of F_{th} obtained by linear

#134586 - $15.00 USD Received 7 Sep 2010; revised 8 Nov 2010; accepted 8 Nov 2010; published 22 Dec 2010
(C) 2011 OSA

regression for a given pulse duration were higher than several fluence values for which a crater was produced. In addition, the mean values of D^2 were clearly not a linear function of $\ln F$ in the 30 fs and 100 fs cases. This behavior was however not so evident in the 7 fs case. We found empirically that the crater diameter squared is in better agreement with the expression:

$$D^2 \propto F - F_{th} \tag{2}$$

Our measurements for stroma are shown in Fig. 4. The dots represent the mean value of D^2 for a given fluence and pulse duration, and the vertical error bars are an estimate of the standard errors of the mean (i.e., $s_F / \sqrt{n_F}$ where s_F is the standard deviation of the measurements for a given fluence F and n_F is the corresponding number of measurements). One can see that the mean values of D^2 align fairly well on the linear regression curves performed on the full data set (i.e., using about 200 measurements) using Eq. (2), for a given pulse duration. Table 2 gives the intercept and slope G and H, respectively, of the regression curves and the correlation coefficient R obtained for stroma.

One observes that the value of R for the 7 fs case in Table 2 is actually lower than the one obtained from Eq. (1) (in parentheses). However, the corresponding value for the slope B (= 49.01 ± 2 μm) is about half the expected value $\ln(10)D_0^2/2$ (= 107.88 ± 10 μm). This is another indication that Eq. (1) is likely not appropriate for stroma. We thus used Eq. (2) for all pulse durations. When considering only the mean values for D^2, the values of F_{th} obtained are similar to those reported in Table 2, namely 0.24 ± 0.16, 0.43 ± 0.25 and 1.56 ± 0.23 J/cm^2 for 7, 30 and 100 fs, respectively, and $R > 0.97$ in all cases. This is our main argument for using Eq. (2) instead of Eq. (1) in the case of stroma.

Table 1. Fused silica: Linear regression coefficients (*A*, *B*) with standard errors, correlation coefficient (*R*), beam diameter (D_0), and threshold fluence (F_{th})

Regression curve: D^2 (μm^2) = $A + B \log F$(J/cm^2)			
	7 fs	30 fs	100 fs
A (μm^2)	–8.97 ± 1.27	–43.10 ± 3.04	–54.72 ± 4.27
B (μm^2)	93.62 ± 2.50	112.01 ± 4.94	96.30 ± 5.66
R	0.9951	0.9895	0.9915
D_0 (μm)	9.2 ± 0.37	8.9 ± 0.36	8.9 ± 0.36
F_{th} (J/cm^2)	1.25 ± 0.02	2.43 ± 0.11	3.70 ± 0.29

Table 2. Stroma: Linear regression coefficients (*G*, *H*) with standard errors, beam diameter (D_0), and threshold fluence (F_{th}). The values of the correlation coefficient (*R*) in parentheses correspond to a fit according to Eq. (1)

Regression curve: D^2 (μm^2) = $G + H F$(J/cm^2)			
	7 fs	30 fs	100 fs
G (μm^2)	–3.12 ± 1.21	–4.98 ± 1.61	–6.83 ± 3.79
H (μm^2·cm^2/J)	13.09 ± 0.63	8.36 ± 0.29	4.64 ± 0.39
R	0.8089 (0.8178)	0.9041 (0.8064)	0.7293 (0.7121)
D_0 (μm)	9.68 ± 0.39	9.1 ± 0.36	9.1 ± 0.36
F_{th} (J/cm^2)	0.24 ± 0.10	0.60 ± 0.21	1.55 ± 0.95

The fact that the crater diameters for stroma do not seem to follow Eq. (1), as for fused silica, is likely related to the inherent characteristics of the two materials. Equation (1) implies that the crater diameter coincides with the thin ring in which a definite fluence F_{th} is obtained in the Gaussian radial intensity profile. Actually stroma is a soft material that may be subject to rearrangement in the area of the crater after the laser shot. This rearrangement may be connected to local dehydration. However, we have not found any substantial argument to explain the linear dependence expressed by Eq. (2). It is possible that Eq. (2) is in fact an approximate representation of a more complicated relation between D^2 and F (as is probably the apparent linear relation between the crater volume and the fluence used in [24]). In fact, a

#134586 - $15.00 USD Received 7 Sep 2010; revised 8 Nov 2010; accepted 8 Nov 2010; published 22 Dec 2010
(C) 2011 OSA

physical justification of the fitting formula is not essential since we are mainly interested in a practical way to extrapolate the data to the point $D^2 = 0$.

The numerical values of F_{th} obtained by extrapolating the regression curves down to $D^2 = 0$ are given in Tables 1 and 2 and are shown in Fig. 5 for the three pulse durations and for corneal stroma and fused silica. The vertical error bars in Fig. 5 were obtained from the standard errors on the parameters of regression curves and correspond approximately to the 70% confidence interval where $D^2 = 0$. The values of the surface ablation thresholds obtained for fused silica are in good agreement with those of [24] (although the definition of the fluence is not specified) and those of [21] (between the high and low threshold fluences) for the three pulse durations considered here. The surface ablation threshold measurements in stroma for 30 fs and 100 fs are also consistent with those of [18,20,25], which were determined from the direct observation of a crater or not, while varying the fluence.

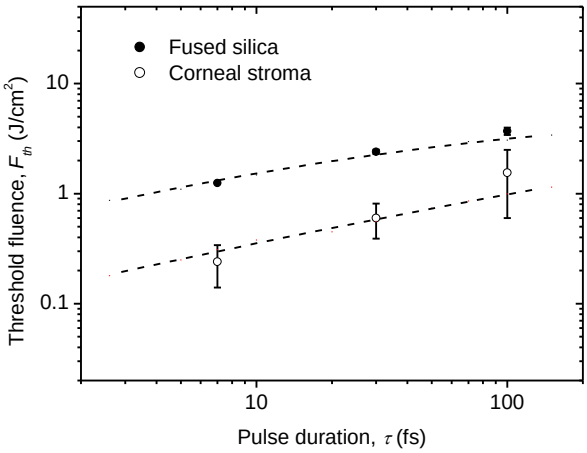

Fig. 5. Surface ablation threshold for corneal stroma and fused silica at 7, 30 and 100 fs. The dashed lines represent fits using the model discussed in [25].

Figure 5 shows that for fused silica, the surface ablation thresholds clearly decrease as the pulse shortens. For stroma, the same tendency is obtained when considering the estimated values without the error bars. Indeed, we find that the ratio between the values of F_{th} for 100 fs and 7 fs are 6.5 for stroma and 3.0 for fused silica. However, when considering the error bars, we can only assert that these ratios are likely (with ~70% confidence) higher than 1.7 for stroma and 2.7 for fused silica. The trends of the threshold fluence from 7 fs to 30 fs and from 30 fs to 100 fs are uncertain for stroma due to large error bars.

3.3 Theoretical model

Figure 5 also shows the fits obtained using a simple theoretical model that includes photoionization, given by the Keldysh theory for solids, and collisional absorption and ionization. The laser propagation and interaction with the medium is modeled by solving the one-dimensional Helmholtz equation with an appropriate dielectric function. Details are given in [25]. We note that the error associated with the use of the Helmholtz equation increases as the pulse duration decreases. We estimate the relative error to be on the order of 10–20% in the 7 fs case at 800 nm.

The fitting parameters of this model are the energy gap U_i and the electron-background collision time for momentum transfer, τ_c. The criterion we used to determine the surface ablation threshold is the smallest fluence for which the energy deposited at the surface of the target reaches the energy density ε_{th} for vaporization of the medium. We define:

#134586 - $15.00 USD Received 7 Sep 2010; revised 8 Nov 2010; accepted 8 Nov 2010; published 22 Dec 2010
(C) 2011 OSA

$\varepsilon_{th} = \chi_e + U_i n_e$, where χ_e is the energy density gained from collisional absorption (inverse Bremsstrahlung) and n_e is the electron density. Electrons recombine with ions and the energy U_i per free electron is eventually converted into heat.

The parameters used for both materials are given in Table 3. For fused silica, we adjusted only the collision time τ_c, which determines collisional absorption, the energy gap U_i = 8.9 eV being know with confidence for high-purity fused silica. For stroma, we used ε_{th} = 2.3 kJ/cm^3 that corresponds to the energy density for vaporization of water. We kept the same value of τ_c as for fused silica and we adjusted the energy gap U_i to fit the measurements.

Table 3. Parameters used in the model of [25] for fused silica and corneal stroma

	Fused silica	Corneal stroma
Linear index of refraction	1.45	1.376
Nonlinear index (cm^2/W)	3.54×10^{-16}	5.7×10^{-16}
Atom density, n_a (cm^{-3})	2.2×10^{22}	3.3×10^{22}
Energy gap, U_i (eV)	8.9	6.0
Collision time, τ_c (fs)	0.7	0.7
Damage threshold, ε_{th} (kJ/cm^3)	27.5	2.3

One observes in Fig. 5 that the surface ablation thresholds for stroma are systematically smaller than those of fused silica. In terms of the model parameters, this is due partly to the lower energy gap U_i, separating the valence band from the conduction band, and partly to the lower energy density ε_{th} required to vaporize the sample surface.

In the framework of this model, the decrease of the surface ablation threshold as the pulse length decreases is essentially due to a more effective photoionization for both materials. This can be seen by considering the contribution of photoionization to ε_{th}, i.e., the fraction $f_{ph} \equiv U_i n_e^{ph} / \varepsilon_{th}$, where n_e^{ph} is the electron density generated only by photoionization at the surface of the material. For fused silica, we find that f_{ph} = 18%, 5% and 0.4% for 7 fs, 30 fs and 100 fs pulses, respectively. The remaining contributions to ε_{th} consists in thermal energy χ_e of the free electrons and of $U_i n_e^{col}$, where n_e^{col} is the electron density associated with collisional ionization. For stroma, the corresponding values for f_{ph} are 39%, 17% and 3%, respectively. This means that the role of photoionization is mainly to provide seed electrons, which then absorb the laser energy via collisions. It should be stressed that the relative contribution of collisional absorption would be smaller for larger values of τ_c. However, for such larger values of τ_c, the threshold fluences would be higher and would not fit the measurements.

To conclude this section, we note that the Keldysh parameter γ, calculated using the threshold fluence and the energy gap U_i, indicates that the photoionization process is mainly tunneling for fused silica for the 3 pulse durations (γ = 0.67, 0.99 and 1.46 for 7, 30 and 100 fs, respectively) while for stroma it is mainly tunneling at 7 fs only (γ = 1.25, 1.63 and 1.86 for 7, 30 and 100 fs, respectively). Here we used the usual rule that γ = 1.5 separates multiphoton and tunneling ionization.

4. Conclusion

A single laser system able of producing intense laser pulses from 7 fs up to several hundreds fs was used to study surface ablation threshold dependence on pulse duration for corneal stroma and fused silica. To our knowledge, this is the first report on laser ablation measurements in biological tissues in the few-cycle regime.

In order to determine the surface ablation threshold, we measured the ablation crater diameter squared D^2 as a function of the laser fluence F and extrapolated the curves obtained by linear regression to zero diameter. We found that for fused silica there is a very accurate linear relation between D^2 and ln F. For stroma, the standard deviation of the measurement was much larger than in fused silica and a fairly good linear relation between the mean values of D^2 and F was observed.

#134586 - $15.00 USD Received 7 Sep 2010; revised 8 Nov 2010; accepted 8 Nov 2010; published 22 Dec 2010
(C) 2011 OSA

The shape of the craters in fused silica are very regular for 7 and 30 fs pulses while some roughness of the crater rim can be noticed at 100 fs. In corneal stroma, the shapes of the crater can show noticeable deviations from a circular shape at 7 and 30 fs. We think that those irregular shapes of the craters and the fact that D^2 seems to be a linear function of F instead of ln F is likely due to material rearrangement after the laser shot.

We estimated that a reduction of the laser pulse duration from 100 fs to 7 fs results in a reduction by a factor greater than 1.7 for the corneal surface ablation threshold and about 2.7 for fused silica. From a simple theoretical model of laser ablation, we conclude that the decrease of the ablation fluence observed for shorter pulses is associated with a more significant contribution of photoionization. However, our model indicates that even for 7 fs pulses, photoionization contributes a fraction less than 50% of the energy density required for ablation.

The threshold fluence for ablation could be further reduced in two different ways: (i) by reducing further the pulse duration at 800 nm, as suggested in Fig. 5, and (ii) by reducing the laser wavelength. Decreasing further the pulse duration at 800 nm from 7 to 3 fs (i.e., nearly a single-cycle pulse [28]) would result in a reduction of the threshold fluence by a factor of ~1.5, as suggested by the dashed lines for both stroma and fused silica in Fig. 5. Reducing the wavelength from 800 nm to 350 nm could also lead to a reduction by a factor ~3 (from 1.5 to 0.5 J/cm^2) for ~100 fs pulses in stroma, as suggested in [25]. Hence, one might think that reducing both the pulse duration and the wavelength should lower further the ablation threshold. However, it should be stressed that the model used in [25] predicts large oscillations in the threshold fluence as a function of the wavelength below 800 nm, which are due to sudden changes in the number of photons required to bridge the effective energy gap between the valence band and the conduction band. This predicted behavior (not yet investigated experimentally) suggests that care should be taken in selecting the wavelength to minimize the ablation threshold fluence. For example, for a pulse duration of 2.8 fs at the central wavelength of 260 nm (i.e., about 3.3 cycles), as achieved recently by Reiter *et al*. [29], our model predicts an ablation threshold of 0.16 J/cm^2 for stroma, which is somewhat smaller than the value of 0.19 J/cm^2 extrapolated from Fig. 5 at 2.8 fs (800 nm). However, for fused silica one rather finds a threshold fluence of 1.07 J/cm^2, which is higher than the value of about 0.89 J/cm^2 extrapolated from Fig. 5 at 2.8 fs (800 nm).

Reducing the laser wavelength would be interesting for studying the underlying physics of laser-induced surface ablation as it can increase the contribution of photoionization. However, for laser dissection in biological tissues, longer wavelengths are more interesting as tissue scattering is reduced, which allows for a better control of the laser focal spot. Hence, few-cycle pulses at longer wavelengths [30,31] may allow reducing both the fluence, thus minimizing damages to the surrounding tissues, and the problematic effects of scattering on the focal spot size.

Acknowledgements

The authors acknowledge the support of the Canada Foundation for Innovation, the Canadian Institute for Photonic Innovations, the Canadian Institutes of Health Research, le Fonds Québécois de la Recherche sur la Nature et les Technologies, the FRSQ Research in Vision Network, the Natural Sciences and Engineering Research Council of Canada, and the Region Provence Alpes Côte d'Azur for funding through the DCOUP project.

#134586 - $15.00 USD Received 7 Sep 2010; revised 8 Nov 2010; accepted 8 Nov 2010; published 22 Dec 2010
(C) 2011 OSA